Photoconductivity studies on nanoporous TiO$_2$/dopamine films prepared by sol–gel method

**G. Valverde-Aguilar · G. Prado-Prone ·
P. Vergara-Aragón · J. Garcia-Macedo ·
Patricia Santiago · Luis Rendón**

Abstract Dopamine was encapsulated into nanoporous amorphous TiO$_2$ matrix by sol–gel method under atmospheric conditions. A second sample was obtained by the addition of the crown-ether 15C5 in this previous sample. Thin films were spin-coated on glass wafers. No heat treatment was employed in both films. All films were characterized using infrared spectroscopy, high resolution transmission electronic microscopy, X-ray diffraction, optical absorption and scanning electronic microscopy. Despite the films prepared with 15C5 were no calcined, a partial crystallization was identified. Anatase and rutile nanoparticles with sizes of 4–5 nm were obtained. Photoconductivity technique was used to determine the charge transport mechanism on these films. Experimental data were fitted with straight lines at darkness and under illumination wavelengths at 320, 400, and 515 nm. It indicates an ohmic behavior. Photovoltaic and photoconductivity parameters were determined from the current density vs. the applied-electrical-field results. Amorphous film has bigger photovoltaic and photoconductive parameters than the partially crystalline film. Results observed in the present investigation prove that the nanoporous TiO$_2$ matrix can protect the dopamine inhibiting its chemical instability. This fact modifies the optical, physical and electrical properties of the film, and is intensified when 15C5 is added.

G. Valverde-Aguilar (✉)
CICATA Unidad Legaria, Instituto Politécnico Nacional,
Legaria 694, Col Irrigación, Miguel Hidalgo, C. P. 11500 Ciudad
de México, Mexico Distrito Federal
e-mail: mvalverde@ipn.mx

G. Prado-Prone · J. Garcia-Macedo
Department of Solid State, Instituto de Física, Universidad
Nacional Autónoma de México, C.P. 04510 Mexico City,
Mexico D.F.

P. Vergara-Aragón
Physiology Department, Faculty of Medicine, Universidad
Nacional Autónoma de México, C.P. 04510 Mexico City,
Mexico D.F.

P. Santiago · L. Rendón
Departamento de Materia Condensada, Instituto de Física,
Universidad Nacional Autónoma de México, C.P. 04510 Mexico
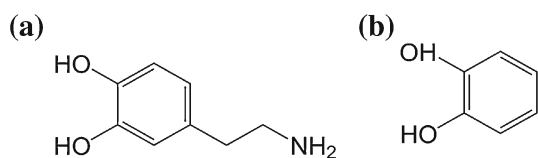City, Mexico D.F.

1 Introduction

Dopamine (DA) (Fig. 1) is an important neurotransmitter in mammalian central and peripheral nervous systems and is also a medicament to cure some neuropsychosis. Enediol ligands, such as DA, have a large affinity for these under-coordinated surface sites, restoring the coordination of Ti atoms to the octahedral geometry and forming ligand-to-metal charge-transfer complexes [1]. Formation of these charge-transfer complexes on TiO$_2$ has been shown to enhance interfacial electron-transfer rates [2, 3]. However, the DA is one of the major sources of reactive oxygen species [4], and it oxidizes very easily when is exposed to the daylight due to its chemical instability. DA contains an unstable catechol moiety with respect to its molecular structure; it can oxidize spontaneously in free radicals and quinones [5–7].

Titanium dioxide (TiO$_2$) is an inexpensive, nontoxic, photostable matrix with redox properties, which are favorable both for oxidation of many organics and for reduction of a number of metal ions or organics in aqueous solution. Although TiO$_2$ is very effective from an energetic point of view, it is relative inefficient in photo-induced reduction and oxidation process [8]. The main energy loss

(a)

(b)

Fig. 1 **a** Molecular structure of dopamine, **b** enediol group of DA

is due to the recombination of charges generated upon excitation of TiO_2, which is manifested as the relatively low efficiency of long-lived charge separation. In addition, because of its large band gap ($E_g = 3.2$ eV), TiO_2 absorbs mainly UV photons. The derivates of dopamine can sensitize TiO_2 nanoparticles to improve the absorption in the visible region making them useful for photocatalysis and solar energy conversion [9].

TiO_2 powder has been developed via sol–gel method [10]. Sol–gel method has been attracting attentions as the typical way to prepare functional materials, e.g., optical glasses, dielectric ceramics, etc. The composition of organic and inorganic compounds can be controlled to optimize their physical properties such as optical and electrical ones [11].

Crown ethers as 15-crown-5 (15C5) contribute to stabilize ions of rare earth as Eu^{2+} by forming the Eu^{2+}(15C5) complex, which enhances the photoluminescent response of the Eu^{2+} ion. This ion is encapsulated by one 15C5 ligand and locates slightly away from the equatorial plane of the central complex cation because of the smaller cavity size of 15C5 ($r = 0.9–1.1$ Å) compared with the divalent europium diameter ($r = 1.09$ Å) [12].

In this work, we described the synthesis, characterization and photoconductivity studies on TiO_2/DA and TiO_2/DA/15C5 films. First, a precursor solution of TiO_2 was prepared by sol–gel method, after DA was dissolved in this solution. It is named TiO_2/DA. A second solution was obtained using the previous one with the addition of 15C5, which named TiO_2/DA/15C5. Both solutions were spin-coated as thin films on glass wafers. No heat treatment was employed in these films. Photoconductivity studies in both films give information about the charge transport mechanism. Transport parameters were calculated. The effect of 15C5 on the optical, physical and electrical properties in these films was studied.

2 Experimental

2.1 Preparation of TiO_2, TiO_2/DA, TiO_2/DA/15C5 and TiO_2/15C5 samples

a) Amorphous TiO_2. TiO_2 precursor solution was prepared by the mixture of Tetrabutylorthotitanate ($Ti(OC_4H_9)_4$) and diethanolamine ($NH(C_2H_4OH)_2$)

which prevent the precipitation of oxides and stabilize the solutions dissolved in 34 ml of ethanol (EtOH). After stirring vigorously for 2 h at room temperature, a mixed solution of deionized water (DI H_2O) and ethanol is added dropwise slowly to the above solution with a pipette under stirring. Finally, Tetraethyleneglycol (TEG) is added to the above solution. The resultant alkoxide solution is kept standing at room temperature to perform hydrolysis reaction for 2 h, resulting in the amorphous TiO_2 solution.

b) TiO_2/DA. To 20 ml of TiO_2 solution prepared in section a), the DA was added in the final stage and the sol was stirred for 15 min at room temperature under darkness. The final chemical composition of this solution was Ti:$NH(C_2H_4OH)_2$:EtOH: DIH_2O:TEG: DA = 1:1:14.1:1:1.028:0.0274.

c) TiO_2/DA/15C5. To 20 ml of TiO_2 solution, 2 ml of 15C5 and the DA were added and stirred for 40 min at room temperature under darkness. The final chemical composition of this solution was Ti:$NH(C_2H_4OH)_2$:EtOH:DIH_2O:TEG:DA:15C5 = 1:1:14.1:1:1.028:0.0274: 0.35372.

d) TiO_2/15C5. To 20 ml of TiO_2 solution, 2 ml of 15C5 was added and stirred for 40 min at room temperature under darkness.

All our solutions were prepared under acidic conditions (pH = 5.0).

Thin films were obtained by the spin-coating technique. The precursor solution was placed on the glass wafers (2.5×2.5 cm^2) using a dropper and spun at a rate of 3,000 rpm for 20 s.

Infrared (IR) studies were done using a Bruker Tensor 27 FT-IR spectrometer. Pellets were made from a finely ground mixture of sample and KBr powder at a ratio of KBr:sample as follows: KBr:DA = 1:0.005, KBr:TiO_2/DA = 1:0.013, KBr:TiO_2/DA/15C5 = 1:0.007 and KBr:TiO_2/15C5 = 1:0.012.

Structural characterization was achieved from conventional high resolution transmission electronic microscopy (HRTEM) by means of a JEOL FEG 2010 FasTem electron microscope with 1.9 Å resolution (point to point). For TEM and HRTEM studies, the sample was suspended in ethanol to disperse the powders and a drop of the sample was deposited on a lacey carbon copper grid as a TEM support.

The structure of the final samples was characterized by X-ray diffraction patterns recorded on a Bruker AXS D8 Advance diffractometer using Ni-filtered CuK$_\alpha$ radiation. A step-scanning mode with 0.02° steps in the 20°–80° range in 2θ and an integration time of 2 s was used.

Optical absorption (OA) spectra were obtained on a Thermo Spectronic Genesys 2 spectrophotometer with ± 1 nm accuracy between 200 and 900 nm.

The thickness of the films was measured using a SEM microscopy Model JSM 5200 CX at 15 kV.

For photoconductivity studies [13], silver electrodes were painted on the sample. It was maintained in a 10^{-5} Torr vacuum cryostat at room temperature to avoid humidity. For photocurrent measurements, the films were illuminated with light from an Oriel Xe lamp passed through a 0.25 m Spex monochromator. Currents were measured with a 642 Keithley electrometer connected in series with the voltage power supply. The applied electrostatic field E was parallel to the film. Light intensity was measured at the sample position with a Spectra Physics 404 power meter.

3 Results and discussion

3.1 IR spectra

Figure 2 shows IR spectra of pure DA powder, and TiO$_2$/DA, TiO$_2$/DA/15C5, TiO$_2$/15C5 films, which were prepared as KBr pellet.

DA was dissolved in DI H$_2$O, its IR spectrum shows several bands located at 554, 600, 752, 814, 878, 935, 962, 1,015, 1,115, 1,150, 1,190, 1,287, 1,342, 1,472, 1,501, 1,601, 2,957, 3,042, 3,146, 3,227 and 3,346 cm^{-1}. These experimental measurements were assigned as Exp. Meas. except the band located at 814 cm^{-1}.

Oxidation products of DA as dopamine quinone (DAQ) and dopaminechrome (DAC) were identified [14, 15] by this technique. DAQ is the first oxidative quinone in the oxidation pathway. After, DAQ spontaneously oxidizes into DAC as shown in Fig. 3.

For TiO$_2$/DA film, the band at 1,653 cm^{-1} is attributable to carbonyl stretching [16]. This band is evidence supporting that DA is oxidized to DAQ [17]. The band centered at 1,456 cm^{-1} is characteristic of the weak C–N bond [18], which appears with the oxidation process of DA. The band at 1,350 cm^{-1} is the v(CC) contribution indicating the formation of DAC. Another evidence of DAQ formation is the band located at 1,288 cm^{-1} assigned to C–O stretching, which disappears during the oxidation process [17]. The bands for oxidation products, DAQ and DAC, are very weak which can indicate that the DA oxidation is minimal.

For TiO$_2$/DA/15C5 film, only the band 1,289 cm^{-1} is assigned to C–O stretching from DAQ. The strong band centered at 1,261 cm^{-1} originates in the C–O-C bonds of TEG [19, 20]. Two bands located at 1,014 and 1,080 cm^{-1} corresponding to the C–O stretching from 15C5 were identified [19]. Several bands correspond to the presence of DA unoxidized were located at 1,505, 1,097, 941 and 818 cm^{-1}. Surprisingly, a poor crystallization in the TiO$_2$ matrix was
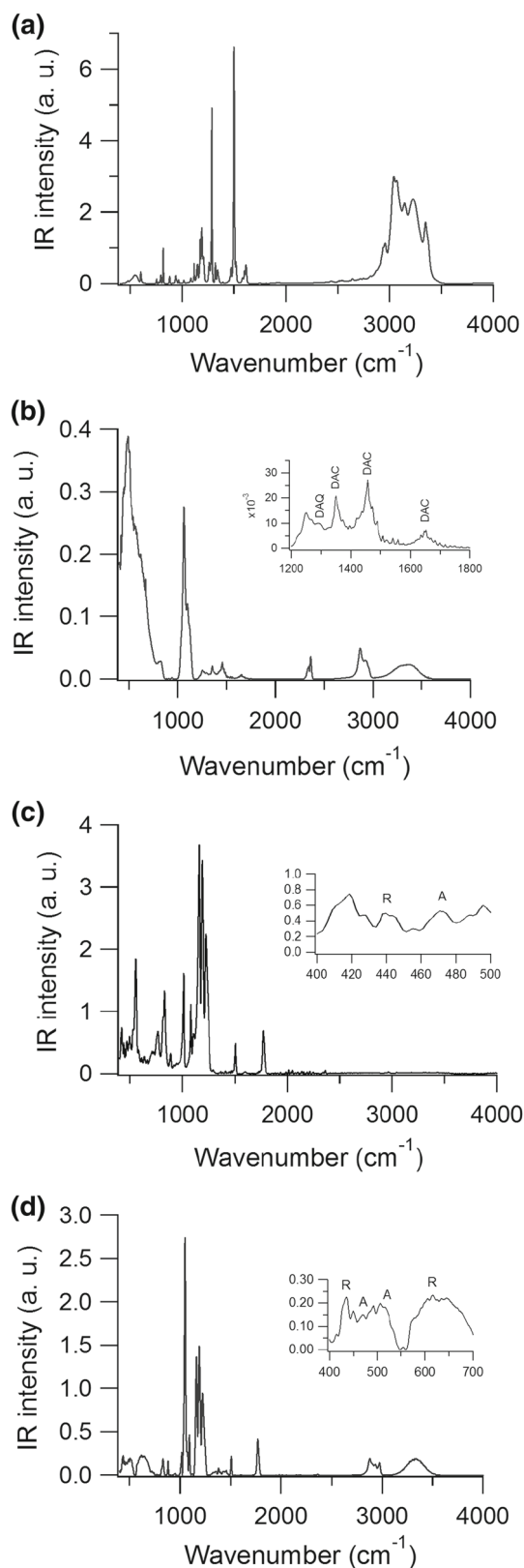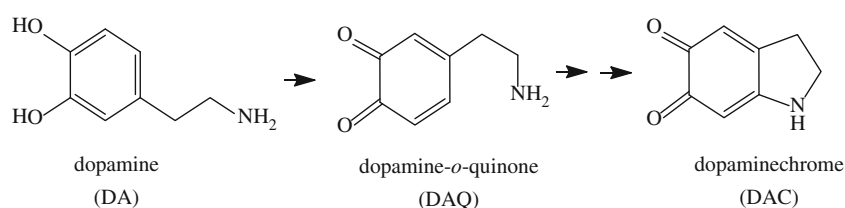

Fig. 2 IR spectra of **a** DA, **b** amorphous TiO$_2$/DA (the inset is a magnification in the region of 1,200–1,800 cm^{-1}), **c** TiO$_2$/DA/15C5 and **d** TiO$_2$/15C5 films (in last two graphs, the *inset* is a magnification in the region of 400–500 cm^{-1}). *A* anatase phase, *R* rutile phase

Fig. 3 Oxidation pathway of
DA

dopamine
(DA)

dopamine-*o*-quinone
(DAQ)

dopaminechrome
(DAC)

detected by typical bands located at 472 and 439 cm^{-1}, which correspond to the $\nu_{Ti-O-Ti}$ stretching vibration for anatase phase and rutile phase, respectively [19, 20]. To verify this effect, the IR spectrum of TiO$_2$/15C5 film was obtained finding similar bands of crystalline phases. This fact is remarkable taking into account that the films prepared with 15C5 were not calcined. Table 1 contains all the vibrations for all films and their assignments.

Therefore, two notable effects were found in these films: (1) the TiO$_2$ matrix protects the DA from the daylight, which inhibits its chemical instability. Besides, the addition of 15C5 increases this inhibition of the DA oxidation, and (2) a partial crystallization was produced in the TiO$_2$ matrix with and without DA when 15C5 is added in the synthesis.

3.2 HRTEM measurements

Figure 4a shows the HRTEM image of the TiO$_2$/DA film. No crystalline phase was detected, which means that this film is amorphous.

In contrast, the Fig. 4b, c shows the HRTEM images from TiO$_2$/DA/15C5 film. These images exhibit some nanoparticles (NPs). The reflections (200) and (220) correspond to anatase phase, and the reflection (210) corresponds to rutile phase. The inset exhibits the diffraction patterns of this reflection. It is in agreement with IR results.

To determine the factor that produces this partial crystallization in the TiO$_2$/DA/15C5 film without any heat treatment, HRTEM studies were done in the TiO$_2$/15C5 film too (Fig. 5). Figure 5a shows a population of NPs with almost spherical shape. Figure 5b, c shows the HRTEM images in which crystalline phases were identified. In Fig. 5b, the spacing between two crystal layers is $d = 0.182$ nm, which is consistent with the reflection (200) corresponding to anatase phase. While, in Fig. 5c, the reflection (200) corresponds to the spacing of $d = 0.206$ nm, which is consistent with rutile phase.

Taking into account a population of these NPs, the average size was calculated. The major axis A and minor length axis B and their respective standard deviations are listed in Table 2.

Table 1 IR frequencies (in cm^{-1}) of DA dissolved in DI H$_2$O; TiO$_2$/DA, TiO$_2$/DA/15C5 and TiO$_2$/15C5 films

| ν_{exp} (cm^{-1})				Assignment	References
DA	TiO$_2$/DA	TiO$_2$/DA/15C5	TiO$_2$/15C5		
–	–	439	435, 617	Rutile	[15]
–	–	472	470, 515	$\nu_{Ti-O-Ti}$ (anatase)	[20]
554	–	553	–	DA	Exp. Meas.
752	–	765	–	DA	Exp. Meas.
814	818	829	–	DA	Exp. Meas., [18]
878	–	887	–	DA	Exp. Meas.
935	941	–	–	DA	Exp. Meas.
1,015	–	1,014	1,015	ν_{C-O} from 15C5	[19]
–	1,097	1,080	1,080	ν_{C-O} from 15C5	[19]
1,150	–	1,159	–	DA	Exp. Meas.
1,190	–	1,188		DA	Exp. Meas.
–	1,250	1,261	1,261	C–O–C bonds (TEG)	[19, 21]
–	1,288	1,289	–	ν_{C-O} (DAQ)	[16, 17]
–	1,350	–	–	ν (CC) (DAC)	[17]
–	1,456	–	–	C=N$^+$ (DAC)	[17]
1,501	–	1,505	–	DA	Exp. Meas.
–	1,653	–	–	Carbonyl stretch. (DAQ)	[16, 17]
–	2,866	–	2,874	C–H vibration	[21]
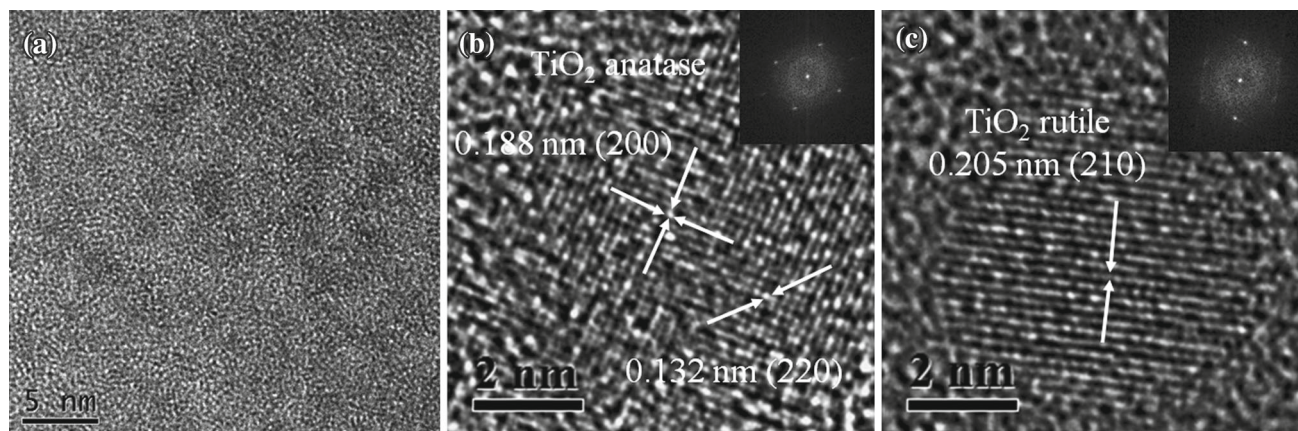
Fig. 4 HRTEM image of **a** amorphous TiO$_2$/DA film; a poor crystallization was exhibit by the presence of **b** anatase phase and **c** rutile phases in the TiO$_2$/DA/15C5 film. The reflections were identified with *white arrows*
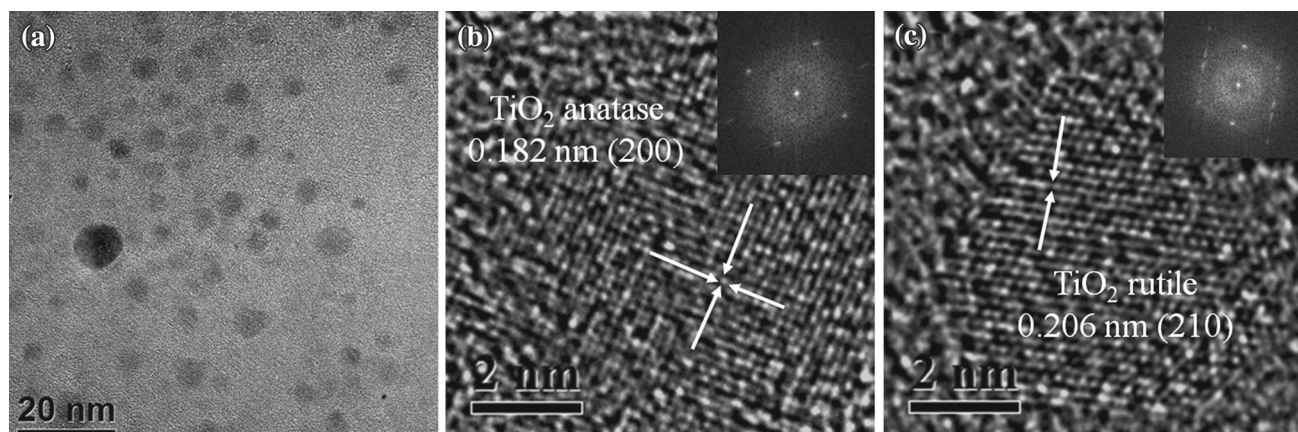

Fig. 5 HRTEM images of TiO$_2$/15C5 sample showing **a** population of NPs; **b** anatase and **c** rutile NPs, respectively. The reflections correspond were identified with *white arrows*

Table 2 Size of NPs in TiO$_2$/15C5 and TiO$_2$/DA/15C5 films

Film	A (nm)	B (nm)
TiO$_2$/DA/15C5 (anatase)	5.5 ± 1.2	5.1 ± 1.0
TiO$_2$/15C5 (anatase)	5.0 ± 1.2	4.7 ± 1.1
TiO$_2$/15C5 (rutile)	4.2 ± 1.4	3.9 ± 1.3

Therefore, the 15C5 acts as structure-directing agent during this slight crystallization of TiO$_2$ matrix in presence of DA, producing nanometric anatase and rutile particles. This partial crystallization of the TiO$_2$ matrix was achieved by the addition of 15C5 as the organic template [22].

No crystalline phases were detected by X-ray diffraction patterns. It means that the crystallization of TiO$_2$ was partial in small areas.

3.3 Optical absorption spectra

Free DA, not oxidized, was dissolved in DI H$_2$O under darkness, and it exhibits a transparent color. Its absorption spectrum (Fig. 6a) shows a strong peak A in the ultraviolet region located at 279 nm. Figure 6b shows the absorption spectra of amorphous TiO$_2$ and TiO$_2$/DA films. Figure 6c shows the absorption spectra of TiO$_2$/15C5 and TiO$_2$/DA/15C5 films. All spectra were taken at room temperature.

Absorption spectrum of amorphous TiO$_2$ film shows an absorption band located at 301 nm. While, for amorphous TiO$_2$/DA film, the absorption spectrum shows two bands located at $\lambda_{max} = 306$ and 440 nm. The first band corresponds to TiO$_2$ absorption, the second one is a very broad absorption band centered at $\lambda_{max} = 440$ nm revealing a red shift.

Similar behavior is observed for the films prepared with 15C5. Absorption spectrum from TiO$_2$/15C5 film shows a
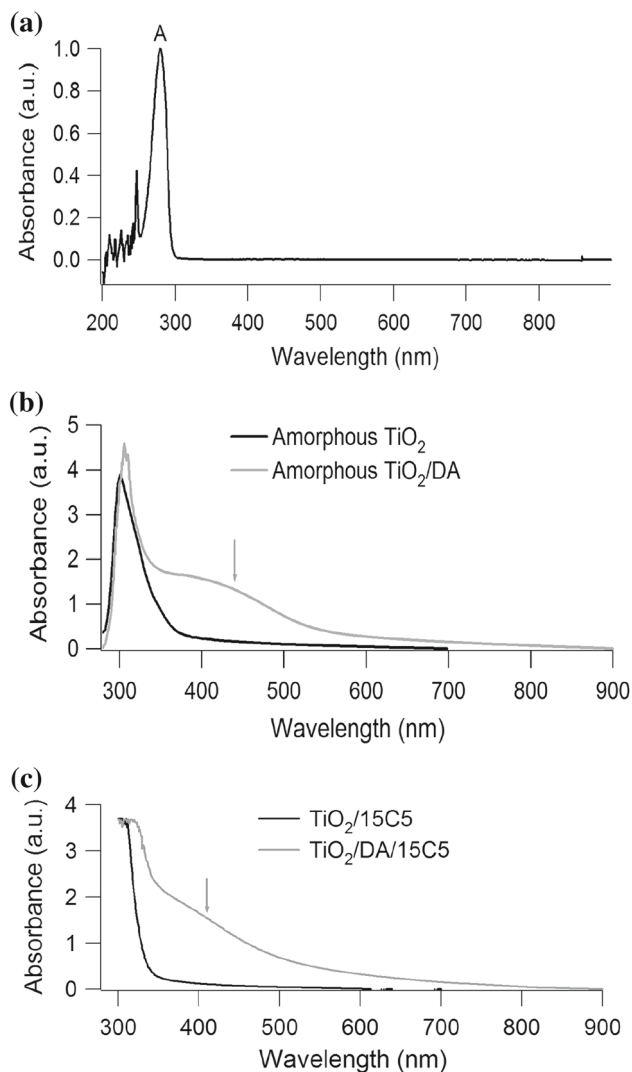
Fig. 6 Absorption spectra of **a** DA dissolved in DI H_2O; **b** amorphous TiO_2 and TiO_2/DA films; **c** TiO_2/15C5 and TiO_2/DA/15C5 films

Table 3 Maximum peaks from absorption bands

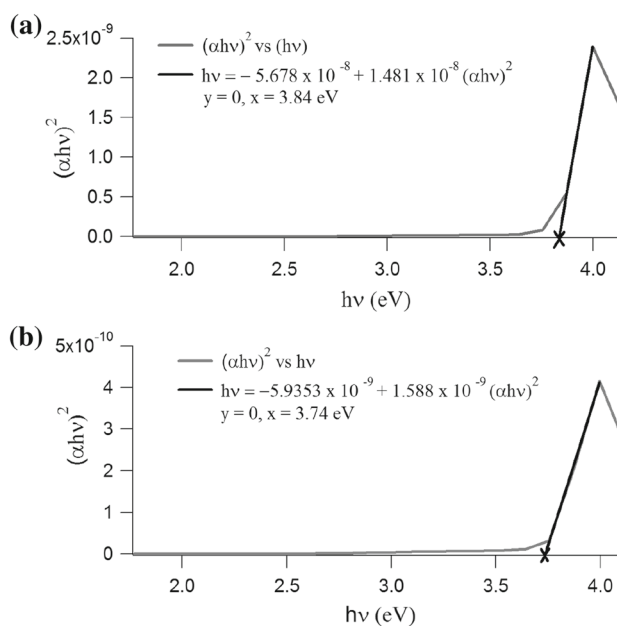| Sample	Maximum absorption peaks		
DA dissolved in DI H_2O	279 nm (4.4 eV)		
Amorphous TiO_2 film		301 nm (4.1 eV)	
Amorphous TiO_2/DA film			306 nm (4.0 eV) 440 nm (2.8 eV)
TiO_2/15C5 film			305 nm (4.1 eV)
TiO_2/DA/15C5 film			310 nm (4.0 eV) 400 nm (3.1 eV)

Fig. 7 Evolution of the $(\alpha h\nu)^2$ vs. $h\nu$ curve of **a** TiO_2/DA film and **b** TiO_2/DA/15C5 film. The value of E_g is marked with a cross

band located at 305 nm. For TiO_2/DA/15C5 film, its absorption spectrum shows two bands located at $\lambda_{max} = 310$ and 400 nm. The first band corresponds to the presence of TiO_2. A broad absorption band located at 400 nm is observed too. This red shift of the maximum peak absorption is less notorious than that for TiO_2/DA film. It is known that the dopamine-functionalized titania NPs show a red shift with decreasing particle size [23]. Therefore, this slight red shift is due to the presence of these NPs which reveals the partial crystallization of TiO_2. Other factor is that surface-trapped electrons exhibit this broad absorption in the visible region under acidic environment [24–27].

Besides, the addition of DA to the precursor TiO_2 and TiO_2/15C5 solutions under acidic environment (pH = 5.0) produces an immediate color change from transparent to red–orange color. This change color indicates the instantaneous formation of the charge-transfer (CT) complex between dopamine and TiO_2, preventing oxidation and formation of reactive intermediates of DA. This stability of the TiO_2 complex with DA is the consequence of bidentate binding of DA [28]. It means that the enediol ligands with two OH groups in *ortho* position (Fig. 1b) undergo unique binding at the surface of TiO_2, resulting in a new hybrid properties of the surface-modified titania NPs [28, 29]. As a result of CT complex, a red shift in the onset absorption for TiO_2/DA and TiO_2/DA/15C5 films is produced.

Table 3 contains all absorption bands for each sample.

The optical band gap (E_g) was determined from the absorption spectra, (Fig. 7) using the equation [30]:

$$(\alpha h\nu)^2 = C(h\nu - E_g), \tag{1}$$

where α is the absorption coefficient, $h\nu$ is the photon energy, E_g is the band gap energy and C depends on the electron–hole mobility.

The $(\alpha h v)^2$ vs. $h v$ plot is displayed in Fig. 7. The value of E_g was determined plotting a tangent line (black solid line) to the curve. For TiO$_2$/DA film, the obtained E_g value is 3.84 eV, and for TiO$_2$/DA/15C5 film this value is 3.74 eV. Both E_g values are marked with a cross. The band gap for TiO$_2$/DA/15C5 film is smaller than that of TiO$_2$/DA film by 0.1 eV; and both values are bigger than those optical band gap reported for amorphous TiO$_2$ (3.5 eV) [31], and for crystalline anatase (3.2 eV) and rutile (3.02 eV) phases [32].

3.4 SEM measurements

The thickness of the films deposited on glass substrate was measured by SEM technique. Figure 8 shows the SEM image for (a) TiO$_2$/DA and (b) TiO$_2$/DA/15C5 films. The thickness average of these films is 5.82 ± 2.08 and 13.75 ± 0.82 μm, respectively. It is due to the fact that the TiO$_2$/DA/15C5 solution is denser than TiO$_2$/DA solution before the deposition as film on glass wafer.

3.5 Photoconductivity studies

Usually Ohm's law under light illumination [13] is given by

$$\vec{J} = \vec{J}_{\mathrm{ph}} + \left(\sigma_d + \sigma_{\mathrm{ph}}\right)\vec{E}, \tag{2}$$

where $\vec{J}_{\mathrm{ph}}$ is the photovoltaic current density, and σ_{ph} is the photoconductivity. When the current densities are assumed

to be parallel to the electric field $\vec{E}$ Eq. (2) becomes into the next one:

$$J = \frac{q\varphi l_0 \alpha I}{h v} + \left(\sigma_{\mathrm{d}} + \frac{q\varphi \mu \tau \alpha I}{h v}\right) E \tag{3}$$

with φ as the quantum yield of charge carrier photogeneration, l_0 as the charge carrier mean free path, α as the sample absorption coefficient, I as the light intensity at the frequency v of illumination, h as the Planck's constant, and τ as the charge carriers mean lifetime. The first term is the photovoltaic transport effect, the second one is the dark conductivity $\sigma_{\mathrm{d}} = en_0\mu$, and the third one is the photoconductivity itself.

Equation (3) can be written as:

$$J = A_1 E + J_0. \tag{4}$$

From the absorption spectra of TiO$_2$/DA and TiO$_2$/DA/15C5 films (Fig. 6), the absorption coefficient (α) was calculated at illumination wavelengths 320 and 400 nm that corresponds to the main maximum absorption bands (Table 3). The wavelength 515 nm is out-absorption region (Fig. 6). Then, the charge transport mechanisms of the films can be compared between the 515 nm wavelength against 320 and 400 nm bands.

Photoconductivity results of both films are shown in Fig. 9. Current density (J) as function of electric applied field (E) on the film was plotted. The experimental data were fitted by least-squares with straight lines at darkness and under illumination. This indicates an ohmic behavior. The linear fits are shown in Table 4.
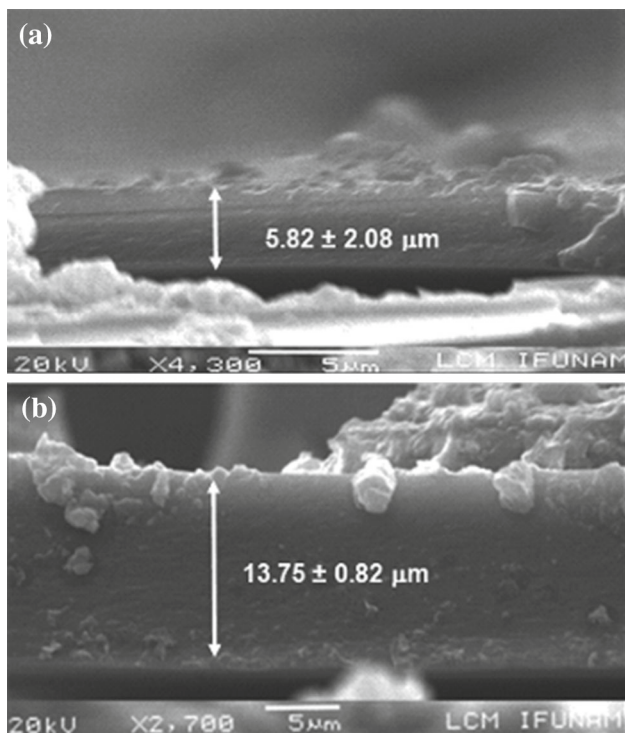

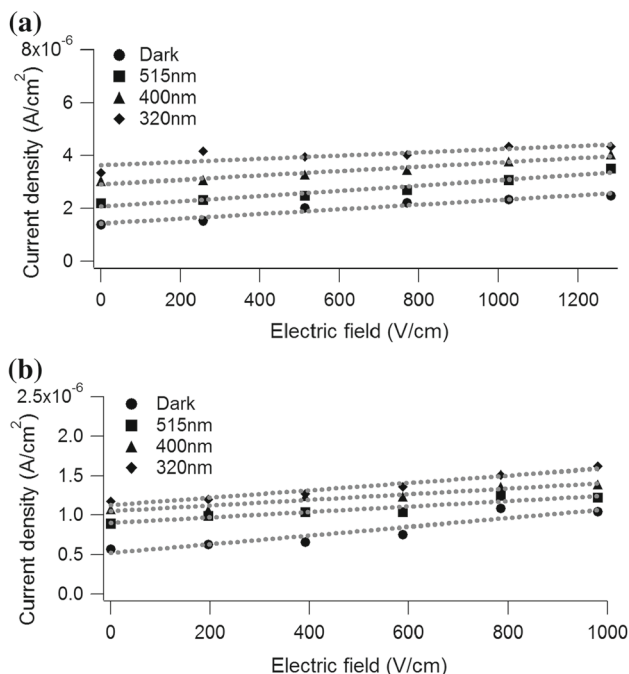Fig. 8 Cross-sectional SEM image of: a TiO$_2$/DA film and b TiO$_2$/DA/15C5 film

Fig. 9 J vs. E curves of TiO$_2$/DA and TiO$_2$/DA/15C5 films. Linear fits correspond to the *dotted lines*

Table 4 Linear fittings of TiO$_2$/DA and TiO$_2$/DA/15C5 films

λ (nm)	Film	A_1	J_0
320	TiO$_2$/DA	3.88×10^{-10}	19.2×10^{-07}
	TiO$_2$/DA/15C5	5.29×10^{-10}	11.1×10^{-07}
400	TiO$_2$/DA	8.20×10^{-10}	29.2×10^{-07}
	TiO$_2$/DA/15C5	4.06×10^{-10}	10.3×10^{-07}
515	TiO$_2$/DA	9.89×10^{-10}	20.8×10^{-07}
	TiO$_2$/DA/15C5	3.94×10^{-10}	8.86×10^{-07}
Darkness	TiO$_2$/DA	8.97×10^{-10}	14.3×10^{-07}
	TiO$_2$/DA/15C5	6.20×10^{-10}	5.11×10^{-07}
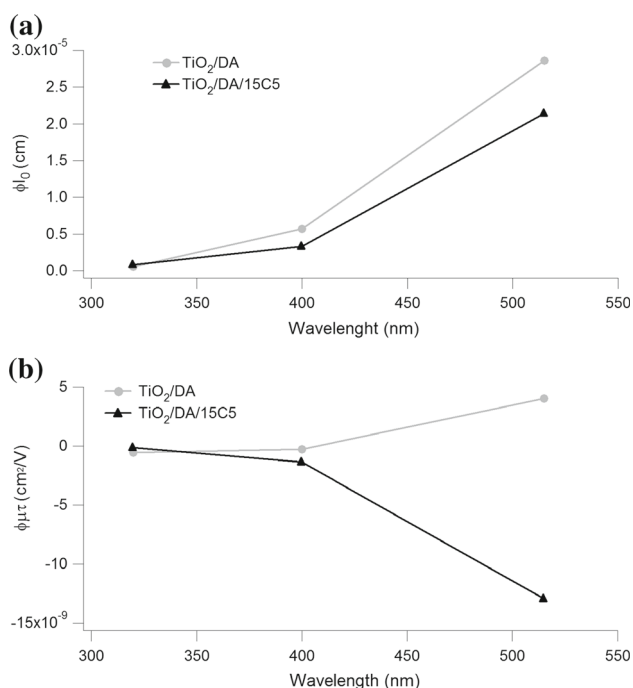
Fig. 10 Photovoltaic and photoconductive parameters vs. wavelength of TiO$_2$/DA and TiO$_2$/DA/15C5 films

For TiO$_2$/DA film, when the illumination wavelength decreases, the slope A_1 decreases. On the contrary, for TiO$_2$/DA/15C5 film the slope A_1 increases. Besides, for TiO$_2$/DA/15C5 film when the illumination wavelength decreases, J_0 increases.

At 400 and 515 nm wavelengths, the slope A_1 and J_0 values for TiO$_2$/DA film are greater compared with those from TiO$_2$/DA/15C5 film. It indicates that the amorphous TiO$_2$/DA film has better photovoltaic and photoconductive properties than the TiO$_2$/DA/15C5 film.

In general, the amorphous TiO$_2$/DA film has a bigger electrical conductivity than the TiO$_2$/DA/15C5 film that can be explained in terms of the band gap (E_g). The E_g values for TiO$_2$/DA (3.84 eV) and TiO$_2$/DA/15C5 (3.74 eV) films enhance 0.64–0.54 eV compared with the $E_g = 3.2$ eV for anatase phase, for what more energy is required to transfer electrons from the valence band (VB) to the conduction band (CB) to generate the charge transport [33]. Besides, the absorption of light having energy greater than the direct band gap (3.75 eV for titanium dioxide) results in the promotion of electrons from the VB to the CB of the metal oxide particle, leaving positively charged holes in the valence band.

On the other hand, when the TiO$_2$/DA/15C5 film is excited with more energetic wavelengths ($\lambda < 327$ nm) than its band gap, the electrons are localized in the conduction band and holes in the valence band. The holes can be located in the surface of the TiO$_2$ preferentially [34], leading to positive charges interacting with the DA directly.

In both films under illumination wavelength at 320 and 400 nm, the slope A_1 is smaller than that measured in the darkness, which means that the films have a high electrical conduction in absence of light. It is known that irreversible oxidation of free DA occurs exclusively with formation of oxygen centered radicals on hydroxyl groups of enediol molecules. In the case when both hydroxyl groups participate in binding to surface Ti atoms, oxidation is reversible and proceeds through carbon centered radicals of the DA aromatic ring. After illumination of the complex TiO$_2$/DA, photogenerated holes localized on carbon centered radicals of the aromatic ring of DA recombine with photogenerated electrons localized on TiO$_2$ particles and irreversible degradation of dopamine does not occur [28] and the charge transport increases. In this case, DA oxidization is very slightly when the film is illuminated because the DA is encapsulated into the TiO$_2$ matrix; and it works as ligand to transfer the charge carriers [32].

With Eq. (4), by measuring I, the dark conductivity and the conductivity under illumination at 515, 400 and 320 nm, and fitting the experimental data by the least-

Table 5 Photovoltaic and photoconductive parameters of TiO$_2$/DA and TiO$_2$/DA/15C5 films

Film	Parameter	515 nm	400 nm	320 nm
TiO$_2$/DA	ϕl_0 (cm)	2.86×10^{-5}	0.57×10^{-5}	0.56×10^{-5}
	$\phi\mu\tau$ (cm^2 V^{-1})	4.01×10^{-9}	-0.29×10^{-9}	-0.58×10^{-9}
TiO$_2$/DA/15C5	ϕl_0 (cm)	2.14×10^{-5}	0.33×10^{-5}	0.08×10^{-5}
	$\phi\mu\tau$ (cm^2 V^{-1})	-12.9×10^{-9}	-1.35×10^{-9}	-0.12×10^{-9}

squares method, the photoconductive ($\phi\mu\tau$) and photovoltaic (ϕl_0) parameters were obtained (Table 5) using the next equations:

$$\phi l_0 = (b_i - b_d)\frac{hc}{e\alpha\lambda I} \qquad (5)$$

$$\phi\mu\tau = (m_i - m_d)\frac{hc}{e\alpha\lambda I} \qquad (6)$$

where b_d and b_i are the intersections of the straight lines in the "y" axes of J vs. E curves under darkness (d) and illumination (i), respectively; m_d and m_i are the slopes of these straight lines under darkness (d) and illumination (i).

Figure 10 shows the photovoltaic and photoconductive parameters vs. wavelength of TiO$_2$/DA and TiO$_2$/DA/15C5 films. In both films, the photovoltaic parameter (ϕl_0) decreases when the wavelength decreases. The ϕl_0 values for TiO$_2$/DA are bigger than those for TiO$_2$/DA/15C5 film. This indicates a strong photovoltaic behavior in the TiO$_2$/DA film.

In TiO$_2$/DA/15C5 film, the photoconductive parameter ($\phi\mu\tau$) value increases when the wavelength decreases. This effect is opposite to that found in the TiO$_2$/DA film. Particularly, at 515 nm wavelength the $\phi\mu\tau$ parameter is bigger TiO$_2$/DA than that for TiO$_2$/DA/15C5 film. It indicates a strong photoconductive behavior in the amorphous film. Therefore, the addition of 15C5 inhibits the charge transport under illumination.

The negative photoconductive parameter in the TiO$_2$/DA/15C5 film is due to the decrease in the number of charge carriers or their lifetime, in the presence of the radiation wavelength [35, 36]. For a negative photoconductor, forbidden gap holds two energy levels in which one is placed between the Fermi level and the conduction band while the other is located close to the valence band. The second state has higher capture cross-section for electrons and holes. As it captures electrons from the conduction band and holes from the valence band, the number of charge carriers in the conduction band gets reduced and the current decreases in the presence of radiation [37].

4 Conclusions

Homogeneous and uniform sol–gel TiO$_2$/DA and TiO$_2$/DA/15C5 films were obtained by spin-coating at room temperature.

DA was embedded into an amorphous TiO$_2$ matrix under acidic conditions to obtain the stable CT complex between DA and TiO$_2$, which was identified in both films by a red shift of the maximum peak absorption.

Oxidation products of DA, DAQ and DAC were found in the TiO$_2$/DA and TiO$_2$/DA/15C5 films by weak infrared bands. It means that DA oxidization is very slightly when the film is illuminated or is exposed to the daylight, because the DA is encapsulated into the TiO$_2$ matrix.

From photoconductivity studies, amorphous TiO$_2$/DA film has better charge transport than the TiO$_2$/DA/15C5 film.

The addition of 15C5 to the TiO$_2$/DA complex produces several effects: (1) inhibits the formation of oxidation products and the charge transport when the film is illuminated; (2) a small red shift of the maximum peak absorption was found; and (3) a partial crystallization in the TiO$_2$ matrix was produced in TiO$_2$/DA/15C5 and TiO$_2$/15C5 films without calcinations.

References

1. T. Rajh, L.X. Chen, K. Lukas, T. Liu, M.C. Thurnauer, D.M. Tiede, J. Phys. Chem. B **106**, 10543 (2002)
2. G. Redmond, D. Fitzmaurice, M. Grätzel, J. Phys. Chem. **97**, 6951 (1993)
3. J. Moser, S. Punchihewa, P. Infelta, M. Grätzel, Langmuir **7**, 3012 (1991)
4. C.-D. Kang, J.-H. Jang, K.-W. Kim, H.-J. Lee, C.-S. Jeong, C.-M. Kim, S.-H. Kim, B.-S. Chung, Neurosci. Lett. **256**, 37 (1998)
5. G. Cohen, R.E. Heikkila, J. Biol. Chem. **249**, 2447 (1974)
6. D.G. Graham, S.M. Tiffany, W.R. Bell, W.F. Gutknecht, Mol. Pharmacol. **14**, 644 (1978)
7. T.G. Hastings, J. Neurochem. **64**, 919 (1995)
8. N.D. Dimitrijevic, L. De la Garza, T. Rajh, Intern. J. Modern Phys. B **23**, 473 (2009)
9. T. Rajh, J.M. Nedeljkovic, L.X. Chen, O. Poluektov, M.C. Thurnauer, J. Phys. Chem. B **103**, 3515 (1999)
10. N. Hafizah, I. Sopyan, Int. J. Photoenergy Article ID 962783, **1** (2009)
11. R. Suzuki, S. Takei, E. Tashiro, K.-I. Machida, J. Alloys Compd. **408–412**, 800 (2006)
12. J. Jiang, N. Higashiyama, K. Machida, G. Adachi, Coord. Chem. Rev. **170**, 1 (1998)
13. G. Valverde-Aguilar, J.A. García-Macedo, V. Rentería-Tapia, M. Aguilar-Franco, Appl. Phys. A **103**, 659 (2011)
14. C.L.L. Pham, S.L. Leong, F.E. Ali, V.B. Kenche, A.F. Hill, S.L. Gras, K.J. Barnham, R. Cappai, J. Mol. Biol. **387**, 771 (2009)
15. Q. He, Z. Zhang, J. Xiong, Y. Xiong, H. Xiao, Opt. Mater. **31**, 380 (2008)
16. X. Wang, B. Jin, X. Lin, Anal. Sci. **18**, 931 (2002)
17. H. Yin, Y. Wada, T. Kitamura, S. Kambe, S. Murasawa, H. Mori, T. Sakata, Y. Yanagida, J. Mater. Chem. **11**, 1694 (2001)
18. P.K. Khanna, N. Singh, S. Charan, Mater. Lett. **61**, 4725–4730 (2007)
19. Y. Djaoued, S. Badilescu, P.V. Ashrit, D. Bersani, P.P. Lottici, J. Sol Gel Sci. Technol. **24**, 255 (2002)
20. S. Musić, M. Gotić, M. Ivanda, S. Popović, A. Turković, R. Trojko, A. Sekulić, K. Furić, Mater. Sci. Eng. B **47**, 33 (1997)
21. Y. Djaoued, S. Adilescu, P.V. Ashrit, J. Sol Gel Sci. Technol. **24**, 247 (2002)

22. C. Berger, R. Gläser, R.A. Rakoczy, J. Weitkamp, Microporous Mesoporous Mater. **83**, 333 (2005)

23. M. Niederberger, G. Garnweitner, F. Krumeich, R. Nesper, H. Cölfen, M. Antonietti, Chem. Mater. **16**, 1202–1208 (2004)

24. D. Dunghong, J. Ramsden, M. Gratzel, J. Am. Chem. Soc. **104**, 2977 (1982)

25. A. Henglein, Berichte der Bunsengesellschaft/Physical Chemistry Chemical Physics **86**, 241 (1982)

26. N.M. Dimitrijevic, D. Savic, O.I. Micic, A.J. Nozik, J. Phys. Chem. **88**, 4278 (1984)

27. A. Safrany, R. Gao, J. Rabani, J. Phys. Chem. B **104**, 5848 (2000)

28. J. Liu, L. De la Garza, L. Zhang, N.M. Dimitrijevic, X. Zuo, D.M. Tiede, T. Rajh, Chem. Phys. **339**, 154 (2007)

29. S. Varaganti, G. Ramakrishna, J. Phys. Chem. **114**, 13917 (2010)

30. J. Tauc, R. Grigorovichi, A. Vancu, Phys. Status Solidi **15**, 627 (1966)

31. D. Rathee, M. Kumar, S.K. Arya, M. Sharma, Key Eng. Mater. **500**, 273 (2012)

32. N. Hafizah, I. Sopyan, Int. Journal of Photoenergy Article ID 962783 (2009)

33. N.M. Dimitrijevic, E. Rozhkova, T. Rajh, J. Am. Chem. Soc. **131**, 2893 (2009)

34. N.M. Dimitrijevic, Z.V. Saponjic, D.M. Bartels, M.C. Thurnauer, D.M. Tiede, T. Rajh, J. Phys. Chem. B **107**, 7368 (2003)

35. V.N. Joshi, *Photoconductivity* (Marcel Dekker, New York, 1990)

36. R.H. Bube, *Photoconductivity of solids* (Wiley, New York, 1981)

37. P. Balamurugaraj, S. Suresh, P. Koteeswari, P. Mani, J. Mater. Phys. Chem. **1**, 4 (2013)